Ultrasound in Med. & Biol., Vol. 26, No. 4, pp. 509–525, 2000

0301-5629/00/$–see front matter

PII S0301-5629(99)00173-8

● *Original Contribution*

THREE-DIMENSIONAL ULTRASOUND IMAGING OF THE ROTATOR CUFF: SPATIAL COMPOUNDING AND TENDON THICKNESS MEASUREMENT

DANIEL F. LEOTTA* and ROY W. MARTIN[†‡]
Departments of *Surgery, [†]Bioengineering and [‡]Anesthesiology, University of Washington, Seattle, WA, USA

(*Received* 13 *July* 1999; *in final form* 14 *December* 1999)

Abstract—Three-dimensional (3-D) volume reconstructions of the shoulder rotator cuff were generated from freehand ultrasound (US) scans acquired with a magnetic tracking system. Image stacks acquired with lateral overlap from multiple acoustic windows were spatially compounded to provide an extended representation of the rotator cuff tendons. A semiautomated technique was developed for measuring rotator cuff thickness from the 3-D compound volumes. Scans of phantoms and volunteer subjects were used to evaluate the accuracy and repeatability of the thickness measurements. For an *in vitro* phantom with known thickness, the mean difference between the true value and the automatic measurements was 0.05 ± 0.28 mm. Thickness measurements made manually from 2-D images and automatically from 3-D volumes were different by 0.03 ± 0.44 mm *in vitro* and −0.06 ± 0.36 *in vivo*. Repeated thickness measurements *in vivo* differed by 0.06 ± 0.36 mm. The 3-D measurement technique offers a promising method for evaluating rotator cuff tendons. © 2000 World Federation for Ultrasound in Medicine & Biology.

Key Words: **Three-dimensional, 3-D, Ultrasound, Spatial compounding, Shoulder, Rotator cuff, Surface extraction.**

INTRODUCTION

The shoulder is a multiaxial ball-and–socket joint that is the most mobile in the body (Markisz 1991). The large range of motion is due to the relatively shallow socket formed by the glenoid cavity of the scapula, into which the humeral head fits. Stability of the shoulder is provided by the rotator cuff, a group of four muscles and tendons (supraspinatus, infraspinatus, subscapularis and teres minor) that arise from the scapula and attach to the tuberosities of the humerus (Matsen and Arntz 1990).

The wide range of movement, heavy use, and dependence on muscle and tendon, rather than a bony socket, for support and strength make the shoulder particularly susceptible to injury. Shoulder pain and weakness can be associated with such pathologies as tendinitis, bursitis, arthritis and rotator cuff tendon tears (Winter et al. 1997). Rotator cuff fiber failure is the most common cause of shoulder pain in patients over 40 y old (Winter et al. 1997). The portion of the rotator cuff that has been found to be most at risk of failure is the section of the supraspinatus tendon approximately 1 cm posterolateral to the biceps tendon (Mack and Matsen 1995). This region is commonly referred to as the "critical zone" of the rotator cuff (Matsen and Arntz 1990; Rafii et al. 1990).

Although some rotator cuff injuries can be attributed to acute trauma, most tears are the result of progressive attrition and degeneration over time (Matsen and Arntz 1990; Rafii et al. 1990). Rotator cuff thinning can precede tears (Mack and Matsen 1995), and is often associated with full- and partial-thickness tears (Benson 1991; van Moppes et al. 1995). Safe and cost-effective monitoring is especially important because patients can often have 10–15 y of chronic shoulder pain before impingement of the tendons and acromion process of the scapula becomes an actual cuff tear (van Holsbeeck and Introcaso 1991).

Ultrasound (US) has become an attractive method for imaging of the shoulder in clinical applications, particularly since the introduction of high-resolution arrays that can image at shallow depths. US has been shown to have high specificity and sensitivity (greater than 90% for each) in diagnosis of rotator cuff tears (Matsen and Arntz 1990). US is particularly useful for performing

Address correspondence to: Daniel F. Leotta, Department of Surgery, University of Washington, Box 356410, Seattle, WA 98195 USA. E-mail: leotta@u.washington.edu

bilateral comparisons of the shoulder, in which paired images from the right and left shoulders are used to confirm pathology (Mack and Matsen 1995). Because the imaging technique presents no known risk to the patient (unlike X-rays), and the cost is relatively inexpensive, the asymptomatic shoulder can be routinely examined for comparison.

Drawbacks to US examination of the shoulder are its long learning curve and operator dependence (Sonnabend et al. 1997; van Moppes et al. 1995). Results can be highly dependent on transducer placement and orientation, due to the complex anatomy of the shoulder. Examination of tendons in orthogonal planes is recommended for diagnosis of tears to assure proper scanhead positioning (Mack and Matsen 1995). However, accurate thickness measurements are difficult to make using 2-D US due to the inherent uncertainty in the slice plane position and orientation (Martin 1996). Diagnosis is limited to real-time interpretation rather than from hardcopy images (Graeme and Jackimczyk 1997; Winter et al. 1997).

Imaging in 3-D provides several attractive benefits compared to 2-D techniques. A 3-D data set provides context for 2-D views: the position of a 2-D sampling plane can be displayed relative to recognizable landmarks in the shoulder. For clinical bilateral shoulder examination, this technique can ensure that comparisons are made at equivalent locations in the two shoulders. The view can be adjusted to ensure that the plane cuts the tendon perpendicular to its surface, to avoid inaccurate results due to oblique slices. A 3-D data set also preserves spatial relationships after an interactive examination has been completed, allowing later review by the examiner, a clinician or a consultant at a remote location. This can enhance confidence that comparisons over time are performed at equivalent sites.

The complex geometry of the shoulder makes it a potentially fruitful area for 3-D spatial compound scanning. Spatial compounding is a technique of combining US image data from multiple views in a single image (Fig. 1). Its use has been suggested for increasing image field of view, enhancing specular reflectors, filling in data gaps, reducing speckle, improving contrast and reducing image artefacts (Kossoff et al. 1978; Robinson and Knight 1981). In the case of the shoulder, the presence of bone makes mental integration of single 2-D slices particularly difficult because large parts of the field of view are shadowed. In addition, tendons have a variable appearance that is strongly dependent on the incidence angle of the acoustic beam, and changes in orientation of muscle capsule and fascia can result in apparent discontinuities when viewed from only one direction. Views from different acoustic windows can fill in shadowed regions and provide more favorable incidence angles for a greater number of structures. By combining these views in 3-D space, a full appreciation of the geometry of the rotator cuff can be attained. The quality of the compounded image, however, is dependent on accurate registration of the regions to be modified. Misregistration due to such factors as scanhead tracking error, beam refraction, speed of sound changes in the beam path and target movement can degrade the quality of the final image.

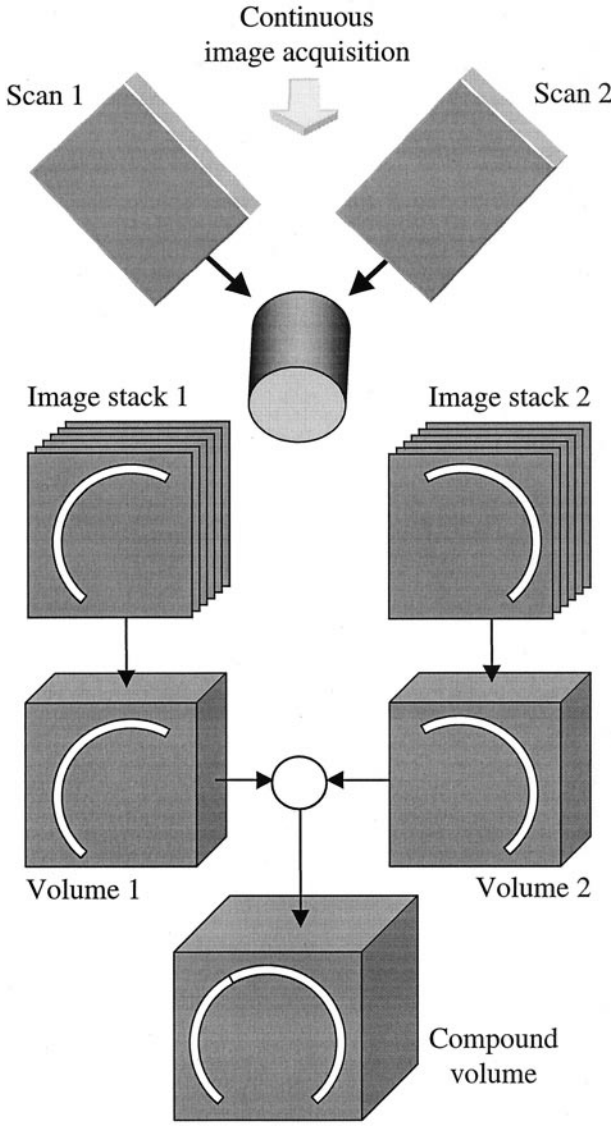

Fig. 1. Schematic of 3-D spatial compounding. Stacks of images captured from different views are converted to volume format and combined. A scan is a set of images captured in one continuous sequence. The image stack captured by a scan is reconstructed into a volume. A compound volume is made up of multiple overlapping registered scans.

The majority of the past work reported in the literature is based on compounding in a single plane (He et

al. 1997; Hernandez et al. 1996; Weng et al. 1997). Recently, however, compounding of 3-D volume data has been introduced. Moskalik et al. (1995) used a mechanical device to translate a scanhead over a region of interest with three different tilt angles in the beam thickness direction to create a 3-D compound volume of the breast. Barry et al. (1997) described a 3-D imaging system based on a magnetic tracking device that demonstrated improved continuity of extracted borders in phantoms. Rohling et al. (1998) also used a magnetic tracking system to acquire freehand scans of a gall bladder from six positions, demonstrating improved image quality, segmentation and volume estimation.

In the current study, 3-D spatial compounding has been applied to the shoulder rotator cuff. A 3-D US scanning system based on magnetic scanhead tracking has been developed (Leotta et al. 1997b) that features flexible and fast data acquisition. Many different orientations of the transducer can be used to acquire data, permitting full interrogation of areas of interest. This method was used to generate 3-D reconstructions of the critical zone of the rotator cuff in healthy volunteer subjects and to make quantitative measurements of tendon thickness over a 3-D region. The accuracy of the method was established by imaging a custom-made phantom *in vitro*. The accuracy relative to 2-D manual thickness measurements and the intrasubject variability of the method *in vivo* were characterized.

METHODS

Three-dimensional imaging

System description. Imaging in 3-D was performed with a standard US imager (HDI 3000, ATL, Bothell, WA) modified with a magnetic tracking system (Flock of Birds, Ascension Technology, Burlington, VT) to register 2-D images in a 3-D coordinate system. All scanning was performed with a linear 10–5-MHz scanhead. The system was calibrated as described in Leotta et al. (1997a). The precision of the system for this scanhead, defined as the rms variability in the measured location of a single-point target imaged with arbitrary scanhead positions and orientations (Leotta et al. 1997a), was 1.4 mm.

The operation of the image capture system is essentially the same as that described in the studies of Leotta et al. (1997b) and Hausken et al. (1998), with synchronized acquisition of image and magnetic tracker data while the scanhead is continuously moved to cover a region of interest. However, the hardware has since been upgraded to a dedicated personal computer with a frame-grabber board (MV-1000, MuTech Corp., Billerica, MA) installed. The system can reliably capture up to 300 images during a single capture cycle. The user enters the capture rate (up to 30 frames/s) and the total number of images to be captured, and then begins the grabbing cycle. Image capture can be initiated at the keyboard or by a hand switch. The current stack of images can either be saved to hard disk or rejected. The upgraded system imposes essentially no limitations on data grabbing, with a 2-GB hard disk available for data storage during an imaging session.

Scanning and reconstruction. A single sequence of images saved from one capture period of the frame grabbing software will be referred to as a scan (Fig. 1). A scan can be characterized by two of the following three parameters: 1. The capture rate in frames/s; 2. the number of frames captured; and 3. the capture time. All scans (both *in vitro* and *in vivo*) were performed at 30 frames/s.

A stack of images converted to a single 3-D data set will be referred to as a volume (Fig. 1). In the volume space, the basic unit is a voxel rather than a pixel. Given a sequence of images and the corresponding position and orientation measurements of the magnetic tracking system, individual 2-D image planes are inserted into a volume space. This step constructs a volume with a regular grid format from the arbitrarily oriented image planes acquired during scanning. The 3-D coordinates of each pixel in the magnetic transmitter's coordinate system are converted to a voxel number *(i,j,k)* using the "nearest neighbor" approach (Trobaugh et al. 1994), which rounds the location to the nearest voxel. In addition, the vector pointing along the image column (the look vector of the incident US beam) is recorded for each interrogated voxel. The use of these vectors will be described below.

The reconstructed voxel size was specified to be a multiple of the pixel size to assure filling of the volume space and to limit the size of the reconstructed volume, which can adversely impact processing and display time. For all reconstructions included below, the voxel size was 5 times the image pixel size. Where multiple pixels land in the same voxel, the mean value of the pixels is assigned to the voxel. All of the software was implemented in the analysis package MATLAB (The MathWorks, Natick, MA).

Compounding. Reconstruction is performed on all scans of a given study to produce separate volumes for each view, which can then be spatially compounded. The combination of multiple views of the shoulder is intended to improve the display of specular interfaces by emphasizing or retaining those views with the most favorable incidence angles. A component of this research project was the development of an enhanced compounding algorithm that weights the contribution to the final volume by the incidence angle in the original view. Resolution and backscatter are expected to be higher

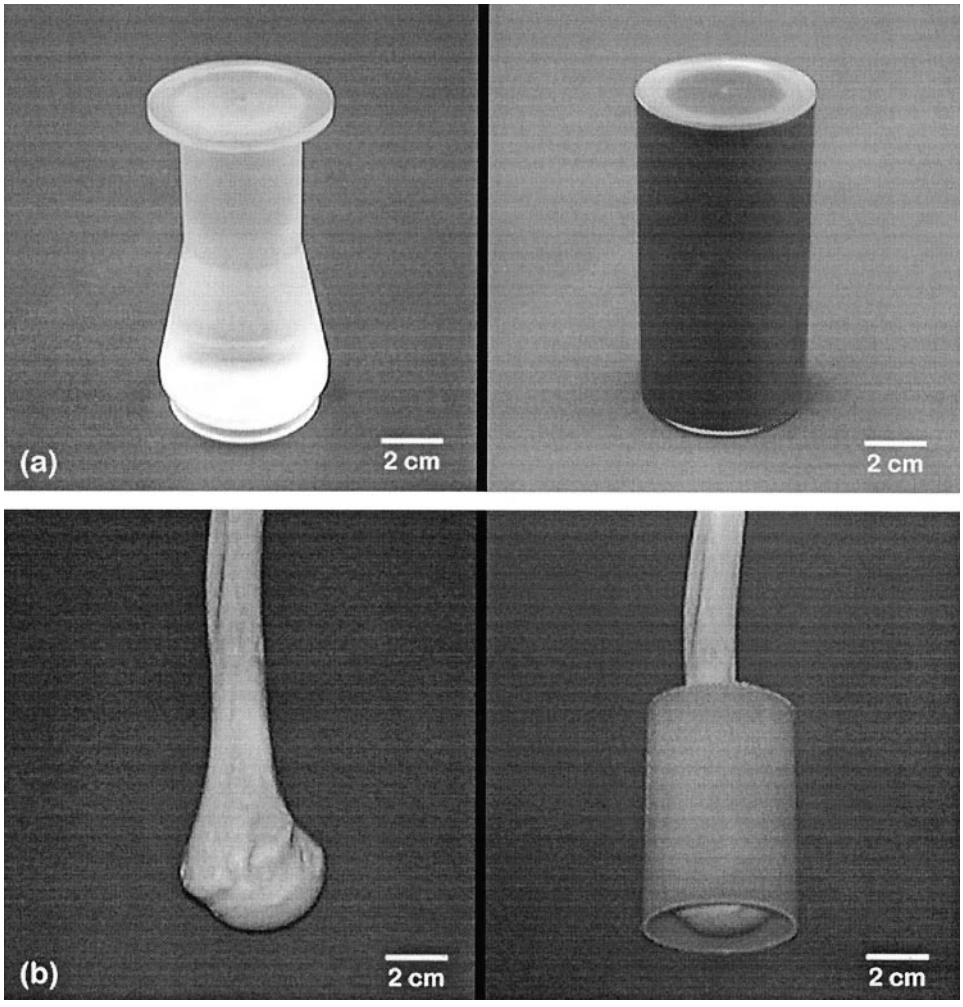

Fig. 2. Photographs of the phantoms used for *in vitro* validation of thickness measurements. (a) The machined plastic phantom with uniform and tapered sections (left). A thin (0.25 mm thick) piece of vinyl was wrapped around the phantom (right) to provide an outer surface for thickness measurements. (b) Bone/cylinder phantom. A human humerus (left) was placed inside a rigid plastic cylinder (right) to simulate a tendon surface from which to make thickness measurements relative to the humeral head.

when the incident beam is closer to normal when it encounters a reflecting surface. Therefore, the compounding algorithm favors regions for which the incidence angle is closer to normal, and rejects data for which the incidence is oblique. This approach reduces intensity variations when views with very different incidence angles are combined. The algorithm and its performance are detailed in Leotta and Martin (1999) and Leotta (1998). All analysis included below was performed on compound volumes generated with this "weighted mean" algorithm.

In vitro thickness measurement

Phantoms. A custom phantom was machined to provide a validation target for 3-D thickness measurements (Fig. 2a). The phantom had a cylindrical section with known diameter, and a tapered section with slope of 0.2 (1 cm radial change/5 cm axial change). The radius of the ends of the phantom was 1 cm greater than that of the cylindrical section. A section of rough vinyl was wrapped around the phantom to provide an outer surface from which thickness measurements were to be made. The vinyl had a thickness of 0.25 mm; therefore, thickness measurements in the uniform section would ideally be 10.25 mm. A human humerus placed inside a thin rigid plastic cylinder measuring 5 cm in diameter was used as a second *in vitro* target (Fig. 2b). In this case, the true distance from the cylinder to the bone was not known.

Scanning and reconstruction. All *in vitro* tests were conducted in a plastic tank filled with a hypertonic saline

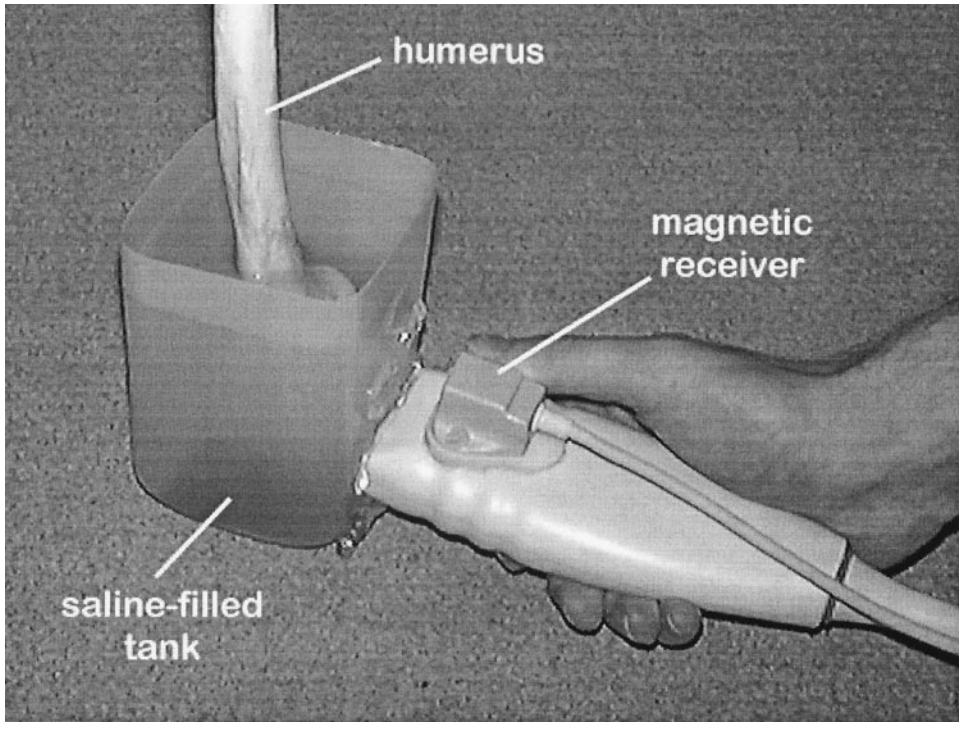

Fig. 3. Photograph of the *in vitro* compound scanning configuration in the laboratory. A human humerus is suspended in a plastic tank filled with hypertonic saline. Images are captured continuously as the transducer is translated along the gel-covered surface of the tank. This configuration allows imaging access from multiple azimuth angles around the target. The magnetic receiver tracks the location and orientation of the scanhead as images are captured; the magnetic transmitter (not shown) is located beneath the wooden table.

solution (4.6% salinity at 22°C). The speed of sound in this solution is equal to the value of 1540 m/s typically assumed for the speed of sound in tissue (Urick 1975). Images were captured while manually translating the scanhead vertically along the tank wall, with each image plane corresponding to a short-axis view of the phantom (Fig. 3). US coupling gel was applied to the walls of the tank to allow smooth movement of the transducer with continuous contact. Scans of each phantom were performed from three windows with lateral overlap. The windows were separated by approximately 45° in the azimuth direction.

Each section (uniform and sloped) of the machined phantom was scanned 3 times from three windows (45° apart), producing three independent compound volume sets. The bone/cylinder phantom was scanned from three windows and reconstructed into compound volumes. Compounding was performed using the weighted-mean algorithm discussed above. The imaging and reconstruction parameters are summarized in Table 1 for both phantoms.

Surface extraction. The thickness measurement technique begins with the extraction of surfaces of interest in the 3-D volume. This is accomplished by applying a surface-detection algorithm to each scan of the compound study, based on gradients in the US beam axial

Table 1. Imaging and reconstruction parameters for thickness measurement scans

Target	Imaging depth (cm)	Images per scan	Number of scans	Pixel size (mm)	Voxel size (mm^3)
Uniform phantom	4.0	180	3	0.1075	0.5376
Tapered phantom	4.0	240	3	0.1075	0.5376
Bone/cylinder	4.0	180	3	0.1075	0.5376
Healthy shoulders	4.0	240	4	0.1075	0.5376
Patient study	4.8	240	5	0.1290	0.6452

All scans were captured at 30 frames/s. The imaging depth is the maximum depth setting of the US instrument during scanning. The voxel scale factor is 5 in all cases (voxel size = 5× pixel size).

direction (look direction). For each scan, the following procedure was executed: 1. Calculate the gradient across each voxel in the direction of the US beam look direction; 2. set all negative values in the gradient volume to zero to isolate the leading edges of the imaged structures; 3. threshold the positive gradient data set to create a binary volume; and 4. apply morphological filtering (thin and prune operations) (Gonzalez and Woods 1993) to sequential 2-D slices extracted in a user-specified direction to remove isolated voxels and reduce the binary regions to a width of 1 voxel.

These steps are demonstrated in Fig. 4 for a cylindrical phantom. Because the gradients are computed along the axial direction of the incident beam, the leading edge of a structure is distinguished by a dark-to–light transition, or positive gradient. Retaining only the positive values, therefore, yields a gradient with a physical significance related to image formation.

Surface normals. The surface-detection step produces a volume of binary data representing the dominant surfaces for a particular view. The normal vectors to these surfaces are calculated using the techniques of principal components analysis (PCA) (Goddard and Kirby 1976). The procedure is as follows: 1. Find all non-zero points in the volume; these points represent the detected 3-D surfaces; 2. at each point, extract a symmetrical $9 \times 9 \times 9$ local volume with the current point of interest at the center; 3. apply PCA (find the eigenvectors and eigenvalues of the covariance matrix of the surface points within the local volume) to the non-zero points in the local volume to find the best-fit plane (in a least squares sense) to the data; and 4. the vector normal to the best-fit plane (the eigenvector with the lowest eigenvalue) is the estimate of the normal to the surface at the point in the center of the current volume of interest.

The local volume size was selected after comparing the accuracy of surface normal angles derived for a cylindrical phantom for size ranging from 5^3 to 11^3 (Leotta 1998). An example of the computed normal vectors is shown in Fig. 4e.

Thickness measurement. The outer surface of the phantoms represents tendon, surrounding a second surface representing bone. To make measurements of the 3-D thickness of the "tendon" overlying the "bone," the surfaces of interest must be distinguished from other surfaces in the volume. Therefore, unique values were assigned to the outer and inner surfaces by applying a connected-components algorithm (Haralick and Shapiro 1992) to the binary surface volume. Bone edges were assigned a value of 20, tendon edges were assigned a value of 10, and unlabeled edges retained their original value of 1.

Each surface point had an associated normal vector that pointed toward the transducer. Thickness measurements were made by extracting a 1-D profile from the reconstructed volume along the line defined by the surface normal vector. The line originated at a point on the tendon surface, and extended away from the transducer through the surface representing the bone. An intensity (grey-scale) profile was extracted by 3-D interpolation along the vector through the labeled edge volume. The thickness was then measured as the distance between the peaks associated with the tendon and bone surfaces. The final result was displayed with AVS software (Advanced Visual Systems Inc., Waltham, MA) as a 3-D isosurface representation of the tendon, which was colored according its thickness in a direction normal to the tendon's surface (Fig. 5). An isosurface connects all voxels of a constant value to generate a surface rendering of a 3-D object.

Validation. The thickness measurements of the uniform section of the machined phantom (Fig. 2a) were compared to the true value. For the tapered section, the measured thickness at each surface point was recorded with its distance along the phantom center axis. A line was fit to the thickness as a function of long-axis position, and the slope of the fit line was compared to the true slope. The difference of the points from a line with the true slope, fit to the data by adjusting the intercept, was also measured.

The second phantom (Fig. 2b) simulates the *in vivo* situation because the distance between the bone and the cylinder was not known. In this case, measurements were validated by comparing manual thickness measurements of original full-resolution 2-D images with those derived automatically from the 3-D compound volume set. This procedure was conducted as follows: 1. Extract a full-resolution 2-D image from the stack of original images; 2. using the image's position and orientation information, extract a corresponding slice from the 3-D surface volume; 3. find the tendon edge points in the extracted slice for which the surface normal vector lies within $\pm 5°$ of the 2-D image plane; 4. for each of these tendon edge points, overlay a line in the 2-D image along the azimuth (in-plane) direction of the surface normal vector; 5. use the mouse to manually locate the tendon edge and bone edge along each line (the automatically-detected edge points are not displayed); 6. calculate the tendon thickness as measured by the observer and compare it with the corresponding automatically measured thickness; and 7. compile statistics for all lines and find the difference between the manual 2-D measurements and the automatic 3-D measurements.

The manual thickness of the tendon was measured as the leading-edge to leading-edge distance from the "tendon" to the "bone" (Fig. 6a). The linear distance in

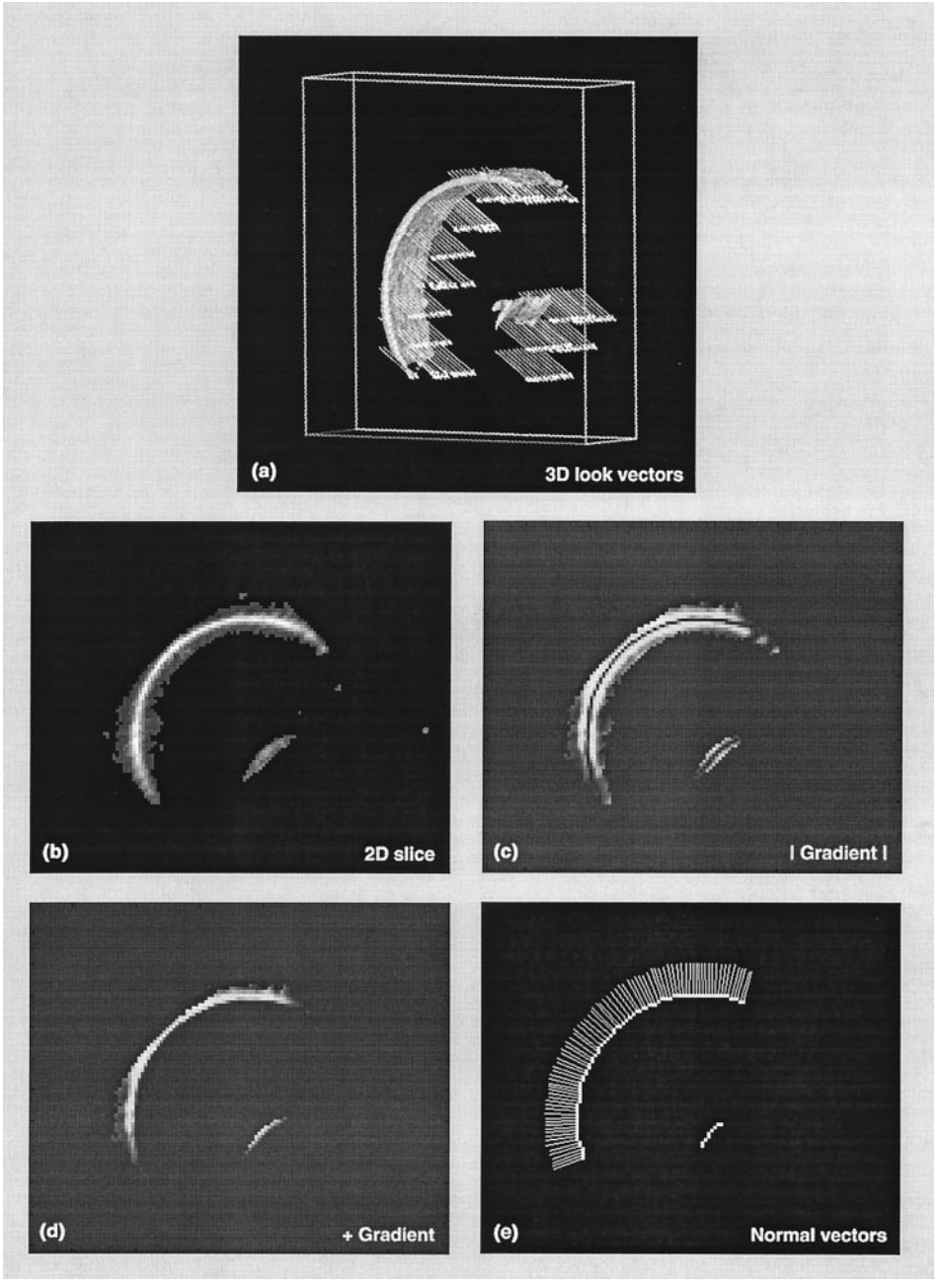

Fig. 4. Example of the surface detection procedure. (a) Subsampled set of look vectors shown in 3-D for a single view of a cylinder. The grey-scale volume data are represented by an isosurface. (b) 2-D slice through the reconstructed volume. (c) Absolute value of the gradient in the look direction, showing gradients on both sides of the object border. (d) Positive gradient values showing the leading edge of the object. (e) Edges derived from the positive gradient after thresholding and morphological filtering. The projections of the vectors normal to the detected surface are superimposed along the surface of the cylinder.

pixels between the two selected points was converted to mm.

In vivo study

Scanning and reconstruction. Data sets of the rotator cuff were acquired to measure tendon thickness *in vivo*. Although clinical scans of the shoulder are normally performed with the subject sitting upright, preliminary tests indicated that subject movement in this position was unacceptable. Additional scans indicated, however, that scanning could be performed with adequate stability of the shoulder when the subject is lying supine

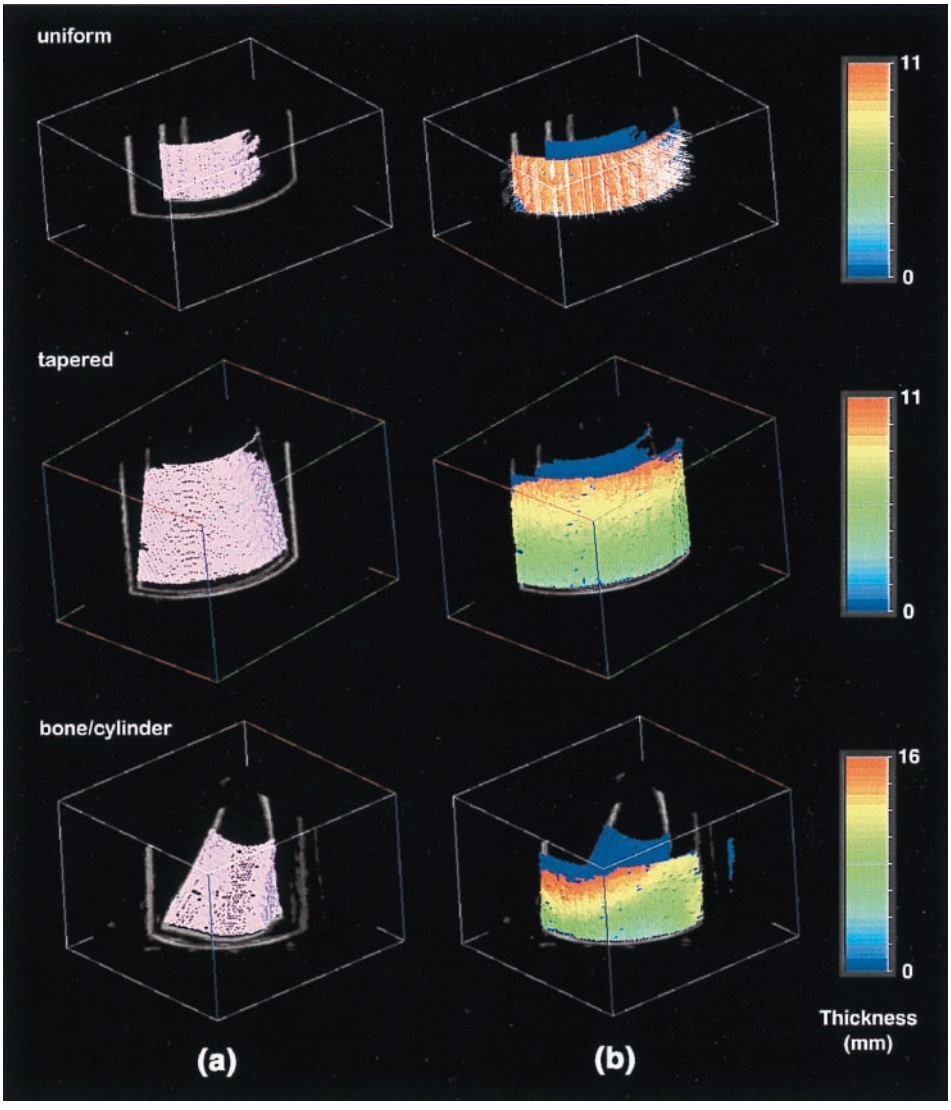

Fig. 5. Isosurface representations of volume reconstructions of the *in vitro* phantoms. (a) Inner surfaces of the uniform, tapered and bone phantoms (top to bottom). (b) Outer surfaces with the distance (in mm) from the outer to the inner surface coded by color. A subsampled set of the normal vectors are superimposed on the outer surface of the uniform phantom (top).

(Fig. 7). Scanning was performed in a laboratory equipped with a nonmetallic bed and mattress to minimize potential interference with the magnetic tracking system. The magnetic transmitter was placed in the cut-out section of a mattress designed for cardiac examinations, placing the transmitter approximately 40 cm from the rotator cuff of the shoulder (Fig. 7). The imaging protocol was approved by the institutional review board; all subjects gave informed consent.

Scanning of the shoulder *in vivo* focused on the anterolateral portion of the rotator cuff, which is the "critical zone" of the supraspinatus tendon, as defined above. Coverage of the region of interest was achieved by a series of three overlapping scans, each starting with a sagittal plane and moving laterally relative to the subject (Fig. 8). A fourth scan, beginning with a transverse plane (lateral approach) and moving in the superior direction, was added for coverage of larger subjects.

For most scans, a square flexible stand-off (Kitecko, 3M, Santé, France) approximately 5-mm thick was placed on the region of the shoulder to be scanned. Coupling gel was placed both between the stand-off and the skin and between the stand-off and the scanhead. The stand-off provided a more uniform coupling of the linear scanhead with the shoulder surface, and permitted smooth movement of the scanhead during image capture.

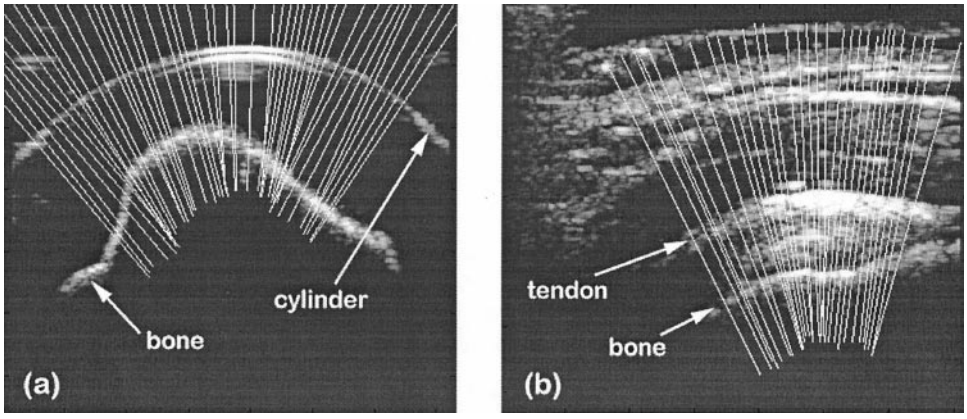

Fig. 6. Full-resolution 2-D images with the vectors normal to the outer surface (cylinder or tendon) superimposed for (a) the bone/cylinder phantom and (b) an *in vivo* rotator cuff. The 3-D normal vectors lie within ± 5° of the 2-D image plane. Manual thickness measurements are made by marking the leading edge of the tendon (or cylinder) and bone along each line.

A demonstration compound data set of the shoulder joint and rotator cuff (acquired from a healthy volunteer subject) is shown in Fig. 9. The subject's arm was held in internal rotation (in front of the body). The scanhead was translated in 3 separate image capture periods to cover the region of the humeral head and supraspinatus tendon lateral and distal to the acromion process of the scapula (lateral and posterior to the biceps tendon). Cov-

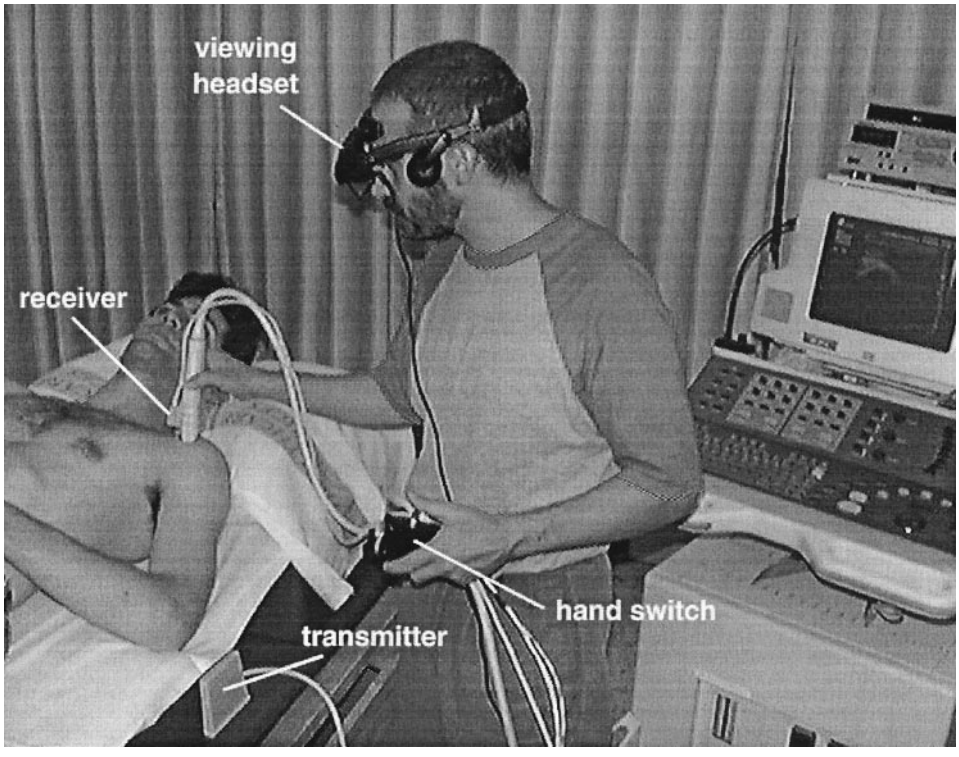

Fig. 7. Photograph of the laboratory configuration for 3-D scanning of the shoulder. The subject lies in the supine position for stability during the scan; a wooden bed is chosen to prevent interference with the tracking system. The magnetic transmitter is placed in the cut-out section of a mattress; the magnetic receiver is mounted on a 10–5-MHz linear scanhead. A headset (Virtual i-glasses®, Virtual i-O, Seattle, WA) allows viewing of the ultrasound images while the scan is being performed. Image capture is initiated by a hand switch connected to a personal computer.

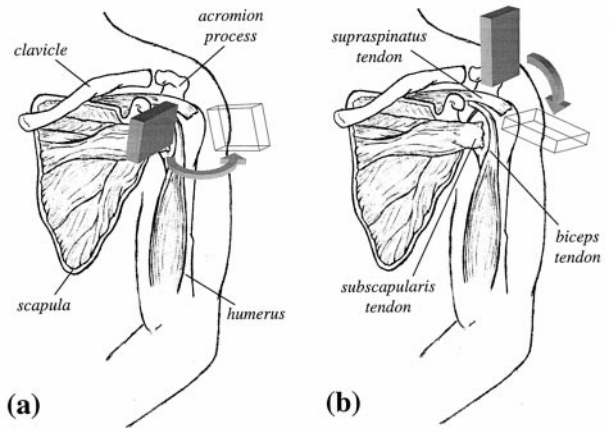

Fig. 8. *In vivo* scanning techniques for the rotator cuff (adapted from Winter et al. 1997). (a) Longitudinal view of the biceps tendon with scanhead movement anterior to posterior. (b) Transverse view of the supraspinatus tendon with scanhead movement superior to inferior. A scan starting between those shown in (a) and (b) provides full coverage of the anterior portion of the rotator cuff. Images are captured at a rate of 30 frames/s as the scanhead is swept from the starting to the ending positions.

erage of the biceps tendon and the superior surface of the acromion process was ensured to provide reference points in the data set. Acquisition of the three scans was completed in 1–2 min. The subject was allowed to breathe normally throughout the study because respiration has little effect on the shoulder in the supine scanning position.

Three healthy volunteers (2 men and 1 woman, ages 25–32 y, heights 163–183 cm) were scanned to quantitatively assess the performance of the thickness measurement technique *in vivo*. For these studies, the subject lay on the mattress in the supine position with the left arm held behind the back in internal rotation and extension. This position provides maximal exposure of sections of the supraspinatus tendon that are normally beneath the acromion process (Winter et al. 1997). The left shoulder was imaged with four separate overlapping scans covering the supraspinatus tendon in the critical zone. The complete scanning sequence was performed 2 more times with the subject remaining in the same position. The entire imaging session (12 scans) was completed in 6–7 min. The result was three independent sets of four scans each.

The shoulder scans were reconstructed using the parameters listed in Table 1. Each of these sets was compounded into a single volume, producing three independent volumes registered in volume space for each subject. A set of four scans of the rotator cuff (of 240 images each) generated 295 MB of data (1 image = 480 × 640 pixels = 307 kB). For a voxel scale of 5, the reconstructed volume was typically on the order of 2 MB (130 × 100 × 150 voxels).

An additional study was performed on a patient with a 2.5-cm tear of the supraspinatus tendon who was examined at the University of Washington Medical Center. The patient had suffered an acute injury to the left rotator cuff approximately 8 months earlier. The right shoulder was also scanned for comparison.

Tendon thickness measurement. Surfaces were extracted from the shoulder sets using the gradient technique described above. As was the case for the phantoms, the surfaces were labeled with unique values for the bone and tendon surfaces. However, because the insertion point of the tendon is included in a typical data set, the bone and tendon edges form a single connected surface. Therefore, points at the junction of the bone and tendon were removed (using a manual editor implemented in MATLAB) to produce two distinct surfaces. Surface labeling was then accomplished using the connected-components algorithm described above. The distance between the tendon and bone was measured along the tendon surface normal vectors.

Validation. The thickness validation procedure described for the bone/cylinder phantom above was applied to the shoulder reconstructions for the 3 healthy subjects. Full-resolution 2-D images were compared to the 3-D volumes at points for which in-plane surface normals were found. The 2-D (manual) and 3-D thickness measurements were recorded along the normal vector directions as above (Fig. 6b).

Repeatability. Tendon thickness measurements were compared for the three scans of each healthy volunteer; the first study was compared with each of the following two studies. Because subject movement between scans was assumed to be negligible, independent measurements of tendon thickness were compared at corresponding surface points across sets. Where the tendon surface points did not directly overlap, thickness measurements were compared at those voxels intersected by the normal vectors of the first surface.

Data analysis

Error in measured thickness for the *in vitro* phantoms was calculated as the mean of the differences from the true thickness. The mean difference in thickness between the 2-D and 3-D methods for both the *in vitro* and *in vivo* tests was also calculated. Intrasubject variability was calculated as the mean of the difference between corresponding measurements for the three compound volumes for each subject. Values are presented as mean ± standard deviation. In addition, the percentage of samples greater than 0.5, 1.0 and 1.5 mm from the true

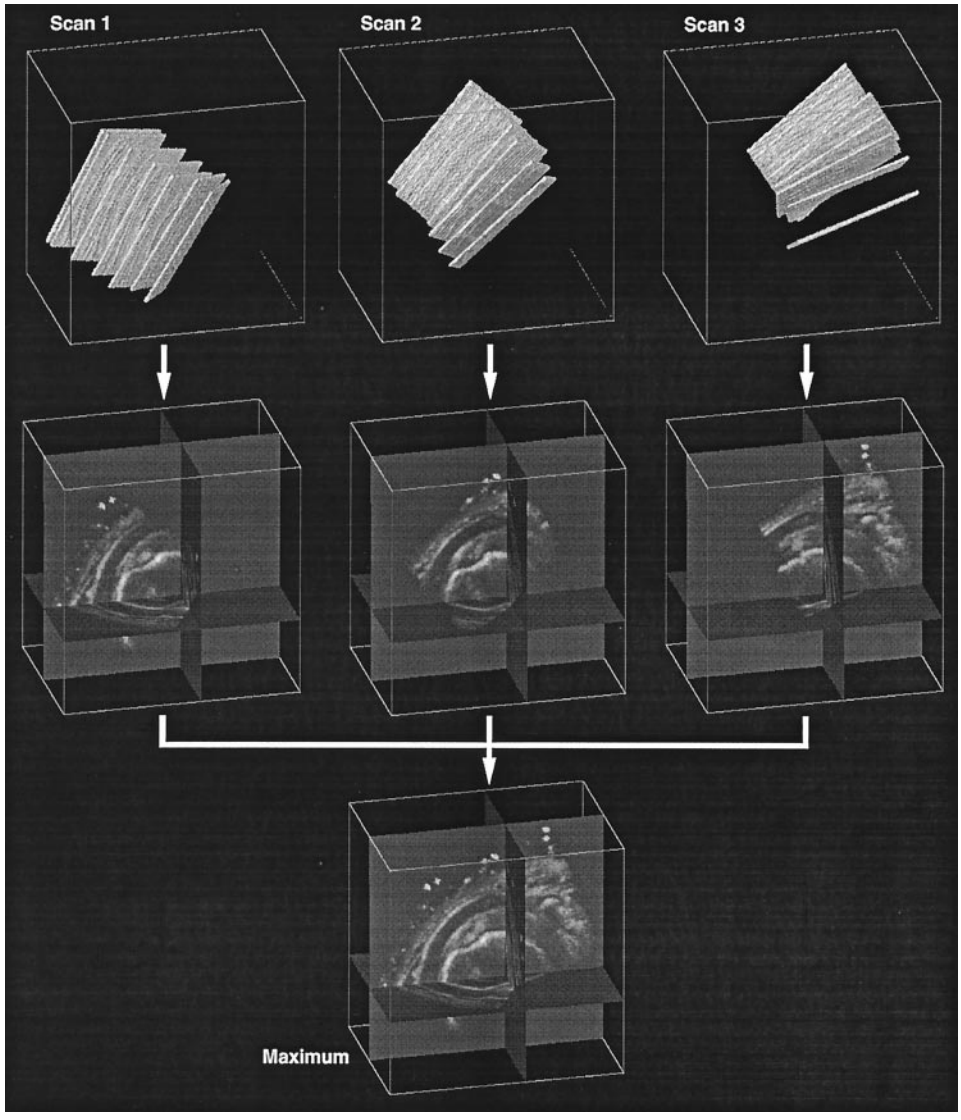

Fig. 9. Example of a compound reconstruction of the rotator cuff imaged *in vivo*. Representative individual image planes of three adjacent scans are displayed as isosurfaces across the top. From left to right, the scan position shifts from anterior to posterior relative to the shoulder. Orthogonal slices through the individual reconstructed volumes for each scan are shown in the middle row. The maximum combination of the three registered scans is shown at the bottom.

value or paired value is reported. This result highlights the extremes of the observed differences.

RESULTS

Uniform in vitro phantom

The differences from the true thickness for the measurements on the uniform section of the plastic phantom are shown in Table 2. The thickness measurements showed no bias from true, with variability less than the size of one voxel. The results for the three repeated scans were nearly identical. Table 3 shows the percentage of samples with error greater than 0.5, 1.0 and 1.5 mm for the three scans combined. Although up to 20% of the samples were between 0.5 and 1.0 mm from true, the number of samples with differences greater than 1 mm was negligible (less than 1% in all cases). This result demonstrates the quantization of the error, where shifts of 1 voxel are between 0.5 and 1.0 mm (voxel size = 0.5376 mm from Table 1).

Tapered in vitro phantom

The thickness measurements on the tapered phantom are summarized in Table 2. The slope of the best-fit line to the data was nearly identical to the ideal slope of

Table 2. Differences from a true or reference value (Δ) for each of the experimental data sets (mean ± standard deviation)

Target	Measured difference (Δ)	Data set	*n*	Mean Δ (mm)
Uniform phantom	3-D thickness − true thickness	study 1	3265	0.04 ± 0.30
		study 2	2937	0.00 ± 0.27
		study 3	2945	0.07 ± 0.31
Tapered phantom	3-D thickness − ideal fit line	study 1	4889	0.00 ± 0.28
		study 2	5709	0.00 ± 0.29
		study 3	5932	0.00 ± 0.28
2-D vs. 3-D *in vitro*	3-D thickness − 2-D thickness	study 1	754	0.03 ± 0.44
2-D vs. 3-D *in vivo*	3-D thickness − 2-D thickness	subject 1	357	−0.02 ± 0.32
		subject 2	348	−0.09 ± 0.34
		subject 3	656	−0.06 ± 0.42
Repeated scans *in vivo*	thickness (study 1) − thickness (study *n*), $n = [2, 3]$	subject 1	3430	0.08 ± 0.40
		subject 2	3051	0.04 ± 0.42
		subject 3	3281	0.03 ± 0.40

Each study represents a volume compounded from multiple scans. The *in vivo* results are based on three studies for each subject. n = number of surface points compared.

0.2 (0.200, 0.203 and 0.202 for the three independent reconstructions). The difference of the raw data points from a line with the ideal slope (fit by adjusting the intercept) had a standard deviation less than the size of 1 voxel. Again, the results for the three repeated scans were nearly identical. The percentage of samples with error greater than 0.5, 1.0 and 1.5 mm are included in Table 3; differences from the fit line are less than 1 mm.

Bone/cylinder in vitro phantom

The differences between the 2-D and 3-D thickness measurements of the bone/cylinder phantom are shown in Table 2. There was no bias of the 3-D measurements compared with the 2-D measurements. The standard deviation was less than the voxel size. Table 3 shows the percentage of sample points with greater than 0.5, 1.0 and 1.5 mm differences between the 2-D and 3-D thickness measurements. Less than 3% of the points were different by more than 1 mm.

Table 3. Percentage of sample points greater than 0.5, 1.0 and 1.5 mm from the reference value for each of the data sets

Data set	% Samples with $\Delta > 0.5$ mm	% Samples with $\Delta > 1.0$ mm	% Samples with $\Delta > 1.5$ mm
Uniform phantom	18.8	0.2	0.0
Tapered phantom	7.4	0.0	0.0
2-D vs. 3-D *in vitro*	24.5	2.6	0.1
2-D vs. 3-D *in vivo*	19.2	0.8	0.0
Repeated scans *in vivo*	32.9	2.5	0.2

The difference measurement Δ for each set was defined in Table 2. The results of three studies were combined for the *in vitro* phantoms (uniform and tapered), and the results for the three subjects were combined in the *in vivo* cases.

In vivo rotator cuff

Views of the compound reconstruction of the rotator cuff with the arm held in front of the body are shown in Figs. 10 and 11. The view of a 2-D slice in the sagittal plane (Fig. 10) demonstrates the registration of the multiple volumes and the increased field of view gained by compounding. The 3-D volume displayed with orthogonal slices (Fig. 11) shows the surrounding anatomical landmarks, which provide a context for viewing and navigating through the reconstructed volume.

An example of rotator cuff reconstructions with bone and tendon surfaces included is shown in Fig. 12, viewed from superior and lateral positions. The superior view of the bone surface clearly shows the greater tuberosity and the bicipital groove of the humeral head. As the detected surfaces are added, the anatomical relationships between the humerus, supraspinatus tendon and surrounding landmarks can be appreciated. The insertion of the supraspinatus tendon on the greater tuberosity of the humerus is particularly well visualized.

Accuracy. The differences between the 2-D and 3-D tendon thickness measurements for the 3 healthy subjects are listed in Table 2. The errors and variability are similar to those observed *in vitro* in the previous section. Table 3 includes the percentage of sample points with greater than 0.5, 1.0 and 1.5 mm differences between the 2-D and 3-D thickness measurements; less than 2% of the points differed by more than 1 mm.

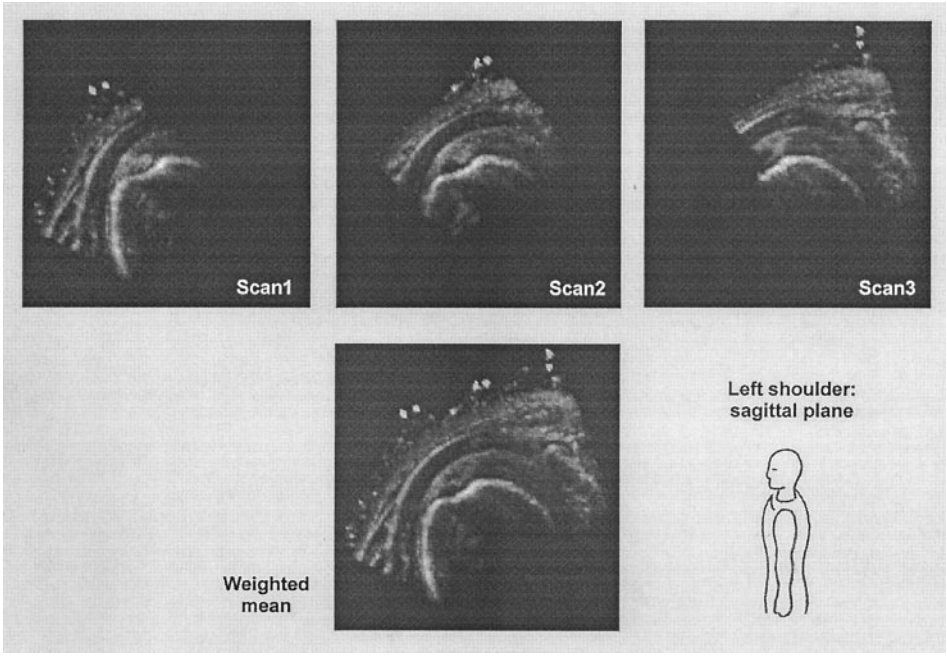

Fig. 10. Example of a compound reconstruction of the rotator cuff. Views from three separate scans (2-D sagittal slices through a 3-D volume) are shown across the top; the compound reconstruction (using the weighted mean algorithm) is shown below. The scan registration and resulting increased field of view are demonstrated.

Repeatability. The differences between the repeated 3-D thickness measurements for the 3 healthy subjects are summarized in Table 2. There was no evidence of a bias in the measurements between scans, and the variability between the sets was on the order of the voxel size. As shown in Table 3, less than 3% of the points differed by more than 1 mm between the repeated scans for each subject.

Patient study. Volume reconstructions of the injured and healthy shoulders of the patient with a rotator cuff tear are shown in Fig. 13. Orthogonal slices through the grey-scale volume data at matching positions relative to the bone are shown at the top of the figure. The flattened surface of the subdeltoid bursa in the region of the tear is clearly visualized, particularly in contrast with the contralateral rotator cuff. Bone and tendon surfaces,

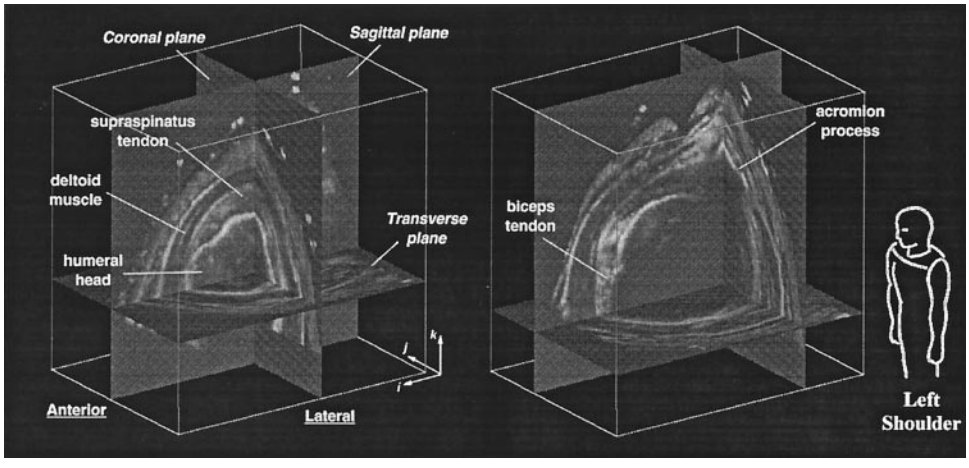

Fig. 11. Orthogonal slices through a compound reconstruction of the rotator cuff imaged *in vivo*. The left shoulder is viewed from the anterolateral position, and the anatomical cutting planes are labeled. In the view on the right, the planes have been moved away from the center to show the biceps tendon and the acromion process of the scapula. (Volume size, $i,j,k, = 135 \times 98 \times 134$ voxels $= 73 \times 53 \times 72$ mm).

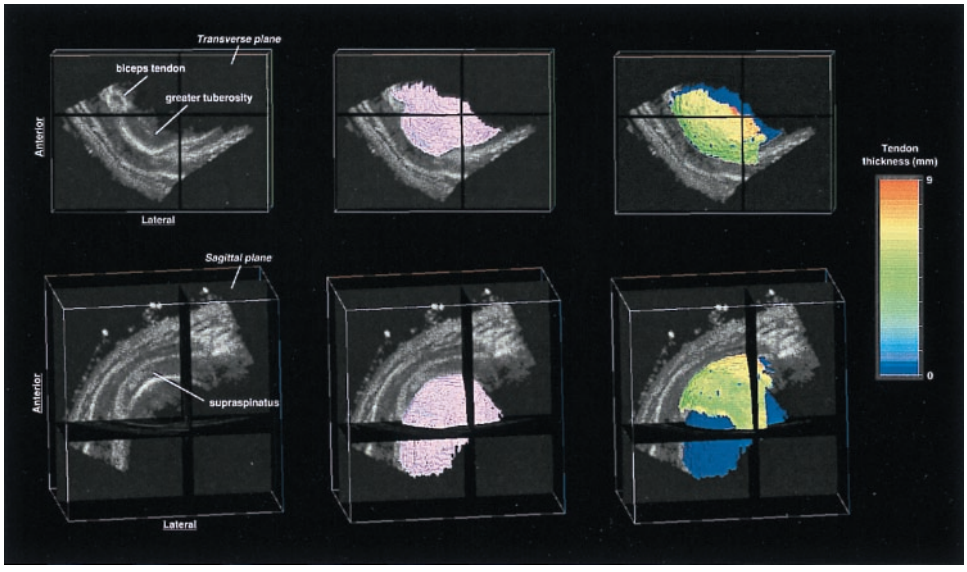

Fig. 12. Reconstructions of the left shoulder *in vivo*. Across the figure are shown orthogonal slices through the grey-scale volume (left), the surface of the humeral head (center), and the tendon surface, with colors representing the thickness above the bone surface measured along the normal vectors (right). Top row: superior-to–inferior view. Bottom row: lateral-to–medial view.

with color-coding of tendon thickness, are shown below the orthogonal slices. The healthy rotator cuff has a nearly uniform thickness of approximately 7 mm over the majority of the imaged region. The injured cuff, however, has a thickness as high as 14 mm (in the region of the retracted end of the tendon), with complete absence of the tendon over the anterior surface of the bone.

DISCUSSION

Compound imaging provides the advantage of an increased field of view when image registration is sufficiently accurate. The freehand system used in this study offers several unique opportunities to investigate compound scanning techniques. Rotational and linear compound scanning techniques (He et al. 1997; Moskalik et al. 1995) are limited to very specific *in vivo* targets. Other systems (Hernandez et al. 1996; Weng et al. 1997) produce only 2-D views. Although He et al. (1997) were able to generate a 3-D volume set, a scan time of 12–15 min was reported. In contrast, flexible scanhead positioning provided by the 3-D freehand system permits full interrogation of different areas of interest. Rapid acquisition times (1–2 min) reduce the potential for motion artifacts when scanning *in vivo*.

This paper has presented quantitative measurements of rotator cuff tendon thickness made from 3-D compound volume reconstructions. Thickness measurements from 2-D images are particularly sensitive to cutting plane orientation. This problem is amplified in the shoulder by the 3-D spherical anatomy of the structures of interest, making 2-D repeatability particularly difficult to achieve. A technique has been introduced that makes measurements automatically from detected surfaces of the bone and tendon, with thickness defined in a direction along a vector normal to the tendon surface. This is a key feature of this approach, in that it provides a standardized thickness measurement defined by the object rather than a viewing plane.

The thickness measurement technique was validated *in vitro* on a machined phantom with known distance between two imaged surfaces. The method demonstrated excellent accuracy and repeatability for both uniform and varying thickness (Table 2). *In vivo* accuracy, however, is more difficult to assess because the true tendon thickness is not known. Therefore, a method was implemented to compare manual 2-D measurements with those returned by automated measurement from the 3-D reconstructed volumes. This approach was validated *in vitro* by imaging a human humerus surrounded by a curved surface. The difference between the user-measured thickness on the original full-resolution images and those returned from the 3-D data sets indicates an excellent agreement between the two methods, with variability less than the size of 1 voxel (Table 2).

Some modifications to the standard clinical procedures for shoulder examination were introduced for 3-D scanning of subjects. First, the subjects were maintained in a supine position for stability of the shoulder during

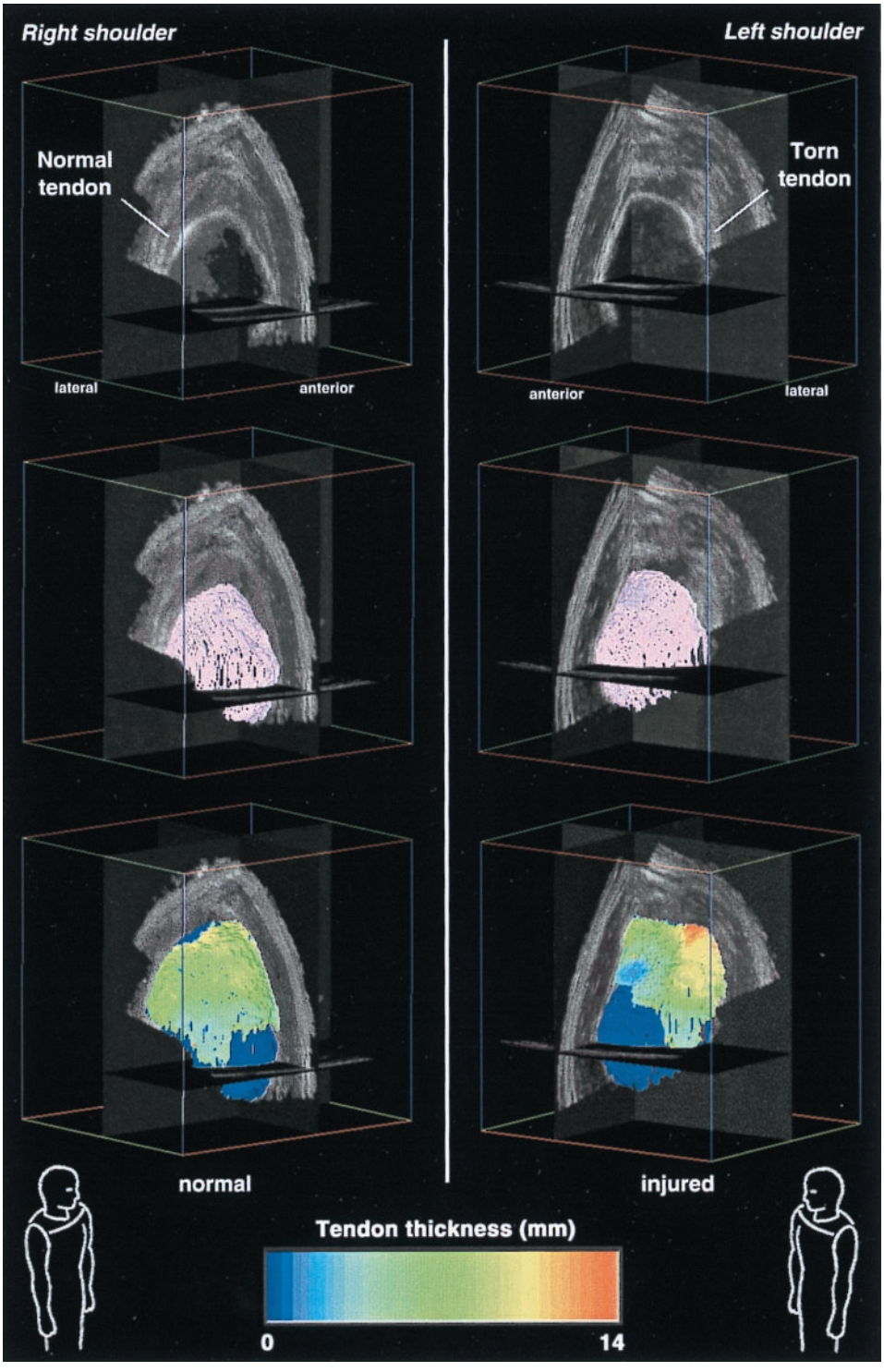

Fig. 13. Rotator cuff reconstructions for a patient with an acute tear of the left supraspinatus tendon. In the top row are shown orthogonal slices through the volume reconstructions of the uninjured shoulder (left panel) and injured shoulder (right panel). Bone surfaces (center row) and tendon surfaces (bottom row) are superimposed on the orthogonal slices. The color map of tendon thickness clearly demonstrates the uniformity of the healthy tendon and the distortion of the torn tendon.

scanning. Any change in shoulder position, whether due to subject movement or as a result of scanhead contact during imaging, would invalidate the 3-D compound reconstructions. An initial scan with a subject seated in an upright position suffered from severe movement artefacts. In over 50 subsequent 3-D scans in the supine position, only 1 reconstruction showed evidence of subject movement. Second, the use of a thin stand-off was introduced after several preliminary scans were degraded by loss of contact between the scanhead and the skin surface. Although large amounts of gel were initially used to aid coupling of the linear transducer with the curved shoulder surface, it was still difficult to maintain complete contact throughout the entire range of motion during the scan. The stand-off helped provide good contact, due to the gel between the stand-off and the skin, and by its deformability on the outer surface. Its smooth outer surface also permitted easy and consistent translation of the scanhead.

Volume reconstructions of the shoulder demonstrate the potential imaging enhancements that 3-D compound scanning can provide. Lateral overlap of the neighboring scans provides extended visualization of the curved structures of the shoulder joint (Fig. 10). Volumes viewed with orthogonal slicing show the critical zone of the rotator cuff within the context of the shoulder anatomy (Figs. 11 and 12). Landmarks (biceps tendon, acromion process) were observed that could guide the placement of slices for thickness measurements.

In vivo thickness measurements compared with full-resolution 2-D images indicated no bias in the 3-D technique, and variability less than the size of 1 voxel. The *in vivo* repeatability study demonstrated excellent agreement between independent scans on the same subject. The sequential repetition of the scans without subject movement provided a reliable set of data with which to assess the variability associated with the data acquisition, reconstruction and analysis. These results indicate the expected measurement variability, given perfect registration between scans. Ideally, similar registration can be achieved in clinical situations over time through automated computer algorithms. Because the humerus is a rigid body, it should provide a good basis for correlation between data sets. In addition, automated separation of the bone and tendon surfaces should be possible using a junction-finding algorithm (Haralick and Shapiro 1992).

With normal rotator cuff thickness ranging from 5 to 10 mm, changes of 1 mm in tendon thickness are considered significant. In current clinical practice, the size of a tear is described by two (approximately) orthogonal length measurements (Wiener and Seitz 1993), and tendon thickness measurements are derived from selected 2-D images. Due to variation in slice positioning, the confidence in observed changes with 2-D US is several millimeters. Because the variability of 3-D tendon thickness measurements was less than 0.5 mm, the technique shows promise for clinical monitoring of tendon thickness over time.

The patient study included in this paper highlights several potential benefits of 3-D US of the shoulder. This patient was in the US clinic for a follow-up visit (approximately 8 months after an acute injury) specifically intended to assess changes in the rotator cuff tear. Visualization of 3-D volume data may offer a more precise means of monitoring morphological changes of the tear. As part of the normal examination, the patient's contralateral shoulder was also scanned. This is an important aspect of the examination because overuse of the uninjured shoulder in compensation for an injury can make the healthy shoulder more susceptible to injury. Three-dimensional thickness measurements may provide a means of accurate assessment of tendon thinning in the healthy shoulder, which can indicate degenerative changes and increased risk of injury in the future. Additional testing on patients is warranted to evaluate the 3-D US imaging method in a clinical environment.

SUMMARY

The techniques presented in this paper offer several enhancements to 2-D measurements of the rotator cuff tendons. 1. Because the thickness is defined relative to the tendon surface, the measurements are not subject to the uncertainty inherent in 2-D imaging, for which the incidence with the tendon surface cannot be strictly controlled. Changes in cutting angle relative to the tendon surface can change the observed thickness in 2-D images. 2. Thickness is recorded over an extended region of the tendon, rather than only at a small number of preselected locations. If other areas should be of interest, the thickness data are available. 3. Because the tendon is displayed within a volume, regional anatomical landmarks enable the extraction of measurements at specific sites of interest. In isolated 2-D images, landmarks such as the biceps tendon or acromion process are not available to ensure that the image is at the precise site of interest. Further clinical evaluation of 3-D rotator cuff imaging is warranted based on initial accuracy and repeatability measurements.

REFERENCES

Barry CD, Allott CP, John NW, Mellor PM, Arundel PA, Thomson DS, Waterton JC. Three-dimensional freehand ultrasound: image reconstruction and volume analysis. Ultrasound Med Biol 1997;23:1209–1224.

Benson CB. Sonography of the musculoskeletal system. Rheum Dis Clin North Am 1991;17:487–504.

Goddard J, Kirby A. An introduction to factor analysis. Norwich: Geo Abstracts Ltd., 1976.

Gonzalez RC, Woods RE. Digital image processing. Reading: Addison-Wesley Publishing Co., 1993.
Graeme KA, Jackimczyk KC. The extremities and spine. Emerg Med Clin NA 1997;15:365–379.
Haralick RM, Shapiro LG. Computer and robot vision. Vol. 1. Reading: Addison-Wesley Publishing Co., 1992.
Hausken T, Leotta DF, Helton S, Kowdley KV, Goldman B, Vaezy S, Bolson EL, Sheehan FH, Martin RW. Estimation of the human liver volume and configuration using three-dimensional ultrasonography: effect of a high-caloric liquid meal. Ultrasound Med Biol 1998;24:1357–1367.
He P, Xue K, Murka P. 3-D imaging of residual limbs using ultrasound. J Rehab Res Dev 1997;34:269–278.
Hernandez A, Basset O, Chirossel P, Gimenez G. Spatial compounding in ultrasonic imaging using an articulated scan arm. Ultrasound Med Biol 1996;22:229–238.
Kossoff G, Garrett WJ, Dadd MJ, Paoloni HJ, Wilcken DEL. Cross sectional visualization of the normal heart by the UI Octoson. J Clin Ultrasound 1978;6:3–9.
Leotta DF. Three-dimensional spatial compounding of ultrasound images acquired by freehand scanning: volume reconstruction of the rotator cuff. Ph.D. dissertation, University of Washington, Seattle, WA, 1998.
Leotta DF, Martin RW. Three-dimensional spatial compounding of ultrasound scans with incidence angle weighting. Proc IEEE Int Ultrason Sympos 1999; (in press).
Leotta DF, Detmer PR, Martin RW. Performance of a miniature magnetic position sensor for three-dimensional ultrasound imaging. Ultrasound Med Biol 1997a;23:597–609.
Leotta DF, Munt B, Bolson EL, Martin RW, Kraft C, Otto CM, Sheehan FH. Quantitative three-dimensional echocardiography by rapid imaging from multiple transthoracic windows: *in vitro* validation and initial *in vivo* studies. J Am Soc Echocardiogr 1997b; 10:830–839.
Mack LA, Matsen FA III. Rotator cuff. In: Fornage BD, ed. Musculoskeletal ultrasound. New York: Churchill Livingstone, 1995:113–133.
Markisz JA. Musculoskeletal Imaging. Boston: Little, Brown and Company, 1991.
Martin RW. Interaction of ultrasound with tissue, approaches to tissue characterization, and measurement accuracy. In: Otto CM, ed. The practice of clinical echocardiography. Philadelphia: WB Saunders, 1996:113–130.
Matsen FA III, Arntz CT. Rotator cuff tendon failure. In: Rockwood CA Jr, Matsen FA III, eds. The shoulder. Philadelphia: WB Saunders, 1990:647–677.
Moskalik A, Carson PL, Meyer CR, Fowlkes JB, Rubin JM, Roubidoux MA. Registration of three-dimensional compound ultrasound scans of the breast for refraction and motion correction. Ultrasound Med Biol 1995;21:769–778.
Rafii M, Firooznia H, Sherman O, Minkoff J, Weinreb J, Golimbu C, Gidumal R, Schinella R, Zaslav K. Rotator cuff lesions: signal patterns at MR imaging. Radiology 1990;177:817–823.
Robinson DE, Knight PC. Computer reconstruction techniques in compound scan pulse-echo imaging. Ultrasonic Imaging 1981;3:217–234.
Rohling RN, Gee AH, Berman L. Automatic registration of 3-D ultrasound images. Ultrasound Med Biol 1998;24:841–854.
Sonnabend DH, Hughes JS, Giuffre BM, Farrell R. The clinical role of shoulder ultrasound. Aust NZ J Surg 1997;67:630–633.
Trobaugh JW, Richard WD, Smith KR, Bucholz RD. Frameless stereotactic ultrasonography: method and applications. Comp Med Imaging Graphics 1994;18:235–246.
Urick RJ. Principles of underwater sound. New York: McGraw-Hill Book Co., 1975:105.
van Holsbeeck M, Introcaso JH. Musculoskeletal ultrasound. St. Louis: Mosby Year Book, 1991.
van Moppes FI, Veldkamp O, Roorda J. Role of shoulder ultrasonography in the evaluation of the painful shoulder. Eur J Radiol 1995;19:142–146.
Weng L, Tirumalai AP, Lowery CM, Nock LF, Gustafson DE, Von Behren PL, Kim JH. US extended-field-of-view imaging technology. Radiology 1997;203:877–880.
Wiener SN, Seitz WH Jr. Sonography of the shoulder in patients with tears of the rotator cuff: accuracy and value for selecting surgical options. AJR 1993;160:103–107.
Winter TC III, Richardson ML, Matsen FA III. Ultrasound of the shoulder. RSNA Electronic J, http://ej.rsna.org/EJ−0−96/TEJ.HTM, 1997.